THE JOURNAL OF PHYSICAL CHEMISTRY C

Article

pubs.acs.org/JPCC

Distinctive Nanoscale Organization of Dicationic versus Monocationic Ionic Liquids

Song Li,[†] Guang Feng,*[,†] José Leobardo Bañuelos,[‡] Gernot Rother,[‡] Pasquale F. Fulvio,[‡] Sheng Dai,[‡,§] and Peter T. Cummings*[,†,∥]

[†]Department of Chemical and Biomolecular Engineering, Vanderbilt University, Nashville, Tennessee 37235, United States

[‡]Chemical Sciences Division, Oak Ridge National Laboratory, Oak Ridge, Tennessee 37831, United States

[§]Department of Chemistry, University of Tennessee, Knoxville, Tennessee 37996, United States

[∥]Center for Nanophase Materials Sciences, Oak Ridge National Laboratory, Oak Ridge, Tennessee 37831, United States

Supporting Information

ABSTRACT: The distinctive structural organization of dicationic ionic liquids (DILs) with varying alkyl linkage chain lengths is systematically investigated using classical molecular dynamics (MD) simulations. In comparison with their counterparts, monocationic ionic liquids (MILs) with free alkyl chains, the DILs with short linkage chains exhibit almost identical structural features regardless of anion types, whereas the long-chain DILs display a relatively insignificant prepeak and low heterogeneity order parameter (HOP), which are accompanied by the less evident structural heterogeneity. Moreover, the predominant role of anion type in the structure of DILs was verified, similar to what is observed in MILs. Finally, the different nanoscale organizations in DILs and MILs are rationalized by the relatively unfavorable straight and folded chain models proposed for the nanoaggregates in DILs and the favorable micelle-like arrangement for those in MILs.

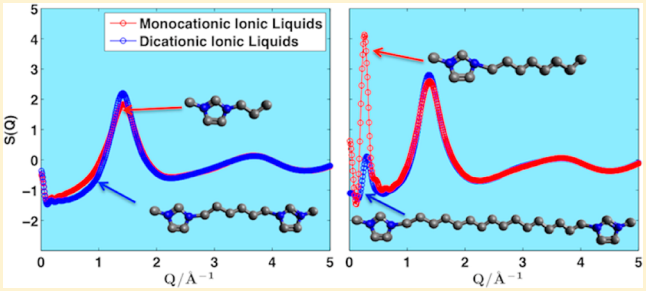

1. INTRODUCTION

Room-temperature ionic liquids (RTILs) are attracting rapidly growing research interest due to their outstanding properties and versatility. In spite of a remarkable increase in the number of RTILs reported, a majority of RTILs under investigation are monocationic ionic liquids (MILs), i.e., having monovalent cations. It has been suggested that the physical and chemical properties of RTILs are mainly determined by the anion due to its diversity, whereas most cations are structurally similar and thus exert less influence on RTIL properties.[1] To expand the diversity of the cation family, a series of imidazolium- and pyrrolidinium-based geminal dicationic ionic liquids (DILs)[2,3] with cations consisting of two identical imidazolium or pyrrolidinium rings linked together by alkyl chains of different lengths are studied. In contrast to cations in MILs, each dication in DILs carries two positive unit charges, and it is structurally symmetrical in most cases. Moreover, subsequent studies reported that DILs, similar to MILs, can be used equally well as catalysts,[4−7] solvents,[8] lubricants,[9,10] and electrolytes,[11,12] especially at high temperatures due to their high stability.[3]

Although the structural and physicochemical properties of MILs have been extensively studied[13−16] and several studies on DILs have been reported,[17−20] the spatial heterogeneity of DILs has yet to be fully explored. The nanoscale organization of MILs has been comprehensively investigated using small-/wide-angle X-ray scattering (SAXS/WAXS),[21−23] small-angle neutron scattering (SANS),[24] and a variety of theoretical simulations.[25−27] The physical significance of the "prepeak" or "first sharp diffraction peak (FSDP)" observed at the low-Q range in the structure functions of MILs with long alkyl chains from both experimental and theoretical work has been debated for decades. Recently, partly as a result of simulation studies, a consensus is emerging that the prepeak is a result of the correlations between anions that are separated by the aggregated long alkyl chains and thus corresponds to anion−anion correlations beyond the first nearest-neighbor shell. The intensity of the prepeak mostly depends on the types of anions whose constituents usually have large X-ray form factors in comparison to the cation alkyl chains.[28] However, relevant studies on this issue have not been reported for DILs. Does linkage chain length impose the same influence on the structural arrangement of DILs as the free alkyl chain in MILs? Do DILs exhibit structural heterogeneity similar to that observed in MILs? What role does the anion play in the structure of DILs? Some answers have been obtained in simulation studies by Ishida[29] and Bodo et al.,[30] in which they reported that the increase of linkage chain length results in the

Received: June 27, 2013
Revised: August 8, 2013
Published: August 8, 2013

ACS Publications © 2013 American Chemical Society

dx.doi.org/10.1021/jp406381g | J. Phys. Chem. C 2013, 117, 18251−18257

emergence of a prepeak at low-Q range in the structure function for DILs. However, the majority of the aforementioned issues are still inviting in-depth exploration.

In this work, a systematic study on DILs 1-alkyl-3-dimethylimidazolium tetrafluoroborate $[C_n(mim)_2](BF_4)_2$ (n = 3, 6, 9, 12, 16) was performed using classical molecular dynamics (MD) simulation. The effects of the linkage chain length on the nanoscale organization of DILs were analyzed in comparison with those of the free alkyl chain length in MILs. The structural heterogeneities resulting from the assembly of long linkage chains in DILs were derived and compared with those formed by long alkyl tail chains in MILs. Moreover, the BF_4 anions were replaced with different alternatives (Br and PF_6) for short- and long-chain dications and monocations, respectively, to study the influence of anion type on the nanoscale ordering. On the basis of these insights, we propose idealized structural models for nanoaggregates formed by the alkyl chains of DILs and MILs that provide a basis for understanding the dissimilarities in the nanoscale segregation of DILs and MILs.

2. SIMULATION METHODS

The force field used for dicationic $[C_n(mim)_2](X)_2$ (n = 3, 6, 9, 12, 16 and X = Br, BF_4, PF_6) was adapted from the all-atom force field developed by Yegagegi et al.,[31] which has been validated and used to predict the densities of DILs with high accuracy compared with experimental data.[3] The force field for monocationic $[C_n mim][X]$ (n = 3, 6, 9 and X = Br, BF_4, PF_6) was taken from the study by Lopes's group.[32] All the hydrogen bonds were constrained during the simulation using the LINCS algorithm,[33] and a 1.1 nm cutoff was used for van der Waals interactions. Long-range electrostatic interactions were processed using the particle mesh Ewald (PME) method.[34] Periodic boundary condition (PBC) was applied in three dimensions. All simulations were performed using the MD package Gromacs.[35] A simulation box consisting of ~1000 ion pairs at low density was initialized at 800 K for 1 ns, followed by a 6 ns equilibration at 450 K in the isobaric−isothermal ensemble. Due to the high melting point (~400 K)[3] of $[C_n(mim)_2](X)_2$, all the simulations were performed at 450 K rather than room temperature to ensure that all ionic liquids are in the liquid phase. The equilibrated box size is in the 8−10 nm range, which is sufficiently large to accurately represent the low-Q peaks above 0.15 Å^{-1} in the structure function. A 2 ns production run generated at 1 bar and 450 K was used for further analysis. The total static structure factors were calculated using the following equation.[36]

$$S(Q) = \frac{\sum_{\alpha\beta} \chi_\alpha \chi_\beta f_\alpha(Q) f_\beta(Q) 4\pi\rho \int_0^{r_c} [g_{\alpha\beta}(r) - 1] r^2 \frac{\sin(Qr)}{Qr} dr}{[\sum_\alpha \chi_\alpha f_\alpha(Q)]^2} \quad (1)$$

where χ_α and χ_β are the fraction of atom species α and β; Q is the wave vector; $f(Q)$ is the form factor of the atom species; $g_{\alpha\beta}(r)$ is the correlation function of atom species α and β; and r_c is the integration cutoff which equals one-half of the simulation box.

The heterogeneity order parameter (HOP) was calculated as well to quantify the effect of the increased alkyl chain on the spatial heterogeneity of DILs and MILs. The following equation is used for the HOP calculation[37,38]

$$h = \frac{1}{N_S} \sum_{i=1}^{N_S} \sum_{j=1}^{N_S} \exp\left(\frac{-r_{ij}^2}{2\sigma^2}\right) \quad (2)$$

where N_S is the total number of sites in the system; r_{ij} is the distance between site i and j corrected by periodic boundary conditions; and $\sigma = L/N_S^{1/3}$ with L being the length of the cubic simulation box. From eq 2, it is indicated that the value of h increases as the spatial heterogeneity is enhanced because the tighter packing of sites results in the smaller r_{ij}, which leads to a larger h.

3. RESULTS AND DISCUSSION

The calculated total static structure factors for DILs $[C_n(mim)_2](BF_4)_2$ are shown in Figure 1, based on which

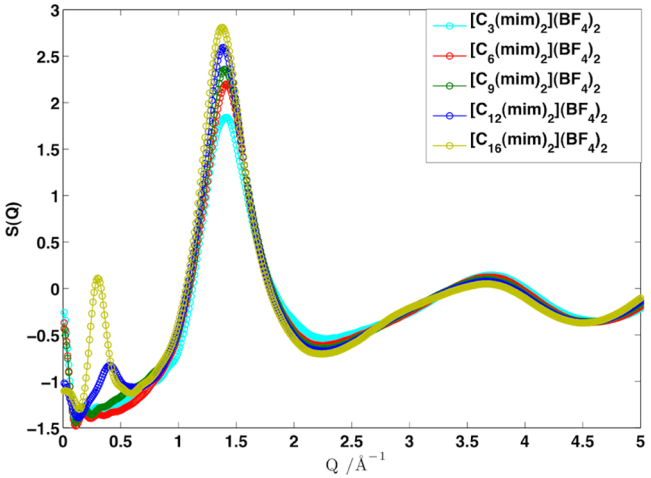

Figure 1. Total static structure factor for dicationic $[C_n(mim)_2](BF_4)_2$ (n = 3, 6, 9, 12, 16).

two findings should be noted. First of all, the intensity of the peak at approximately 1.4 Å^{-1} increases with the elongation of the linkage chain length and shifts to low-Q range. According to previous studies of MILs,[39−41] the peak located at 1.4 Å^{-1} is mainly due to the interaction between co-ions, that is, cation−cation or anion−anion interactions. The chain-length-dependent increase of the peak intensity implies a strengthened correlation between co-ions, and the peak shift toward the low-Q range corresponds to the increased distance between co-ions. The partial structure factors shown in Figure 2 reveal that the peak located at 1.4 Å^{-1} in Figure 1 mainly results from the cation−cation correlations (Figure 2a), which displays the enhanced peak intensity as well as shifted peak positions toward low-Q as the linkage chain length increases from C3 to C16. By focusing on subcomponents (i.e., the head and chain in the dication) of the cation−cation correlation as shown in Figure 2e,f, we see that the increased intensity of the peak at 1.4 Å^{-1} is dominated by the linkage chain−chain correlations (Figure 2f). The enhanced chain−chain interaction is also confirmed by the radial distribution functions (RDFs) of linkage chains shown in Figure S1d in the Supporting Information (SI), where, in contrast to the ring−ring, ring−anion, and anion−anion RDFs, the first peak of the chain−chain RDF increases significantly with increasing linkage chain length. The other phenomenon noticed at the low-Q range is the rise of the prepeak located at

dx.doi.org/10.1021/jp406381g | J. Phys. Chem. C 2013, 117, 18251−18257

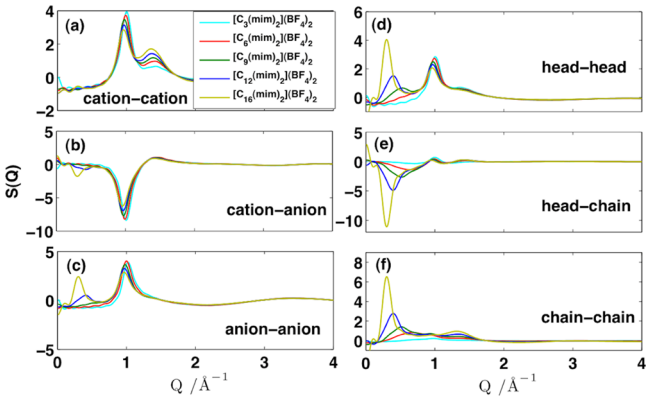

Figure 2. Structure functions of $[C_n(mim)_2](BF_4)_2$ (n = 3, 6, 9, 12, 16) contributed by cation–cation (a), cation–anion (b), and anion–anion (c) correlations and the cation head–head (d), head–chain (e), and chain–chain (f) subcomponents of cation–cation correlations for $[C_n(mim)_2](BF_4)_2$.

0.3 Å^{-1} as the chain length increases, which is similar to that observed in MILs with long alkyl tails.[23,39,40,42−44]

Figure 2c verifies that the presence of a prepeak is mainly attributed to the anion–anion correlation, similar to the conclusion drawn from studies on MILs.[28,45] Although Figure 2f presents the enhanced chain–chain interactions as chain length increases, the chain–chain interactions do not contribute to the increased prepeak intensity directly. Nevertheless, the increased alkyl chains occupy more space, which leads to the enhanced anion–anion correlations and eventually the presence of the prepeak. Moreover, the aggregate composed of long linkage chains is shown in the snapshots of Figure 3, suggesting that DILs as well as MILs manifest enhanced structural heterogeneity with the elongation of chain length. On the basis of the above findings, it seems fair to conclude that the increased linkage chain in DILs plays a similar role as the alkyl chain in MILs. However, there are significant dissimilarities in the nanoscale structure between DILs and MILs as the elongation of the chain length. On the basis of visual inspection of Figure 3, it is apparent that the aggregate sizes formed in MILs ($[C_6mim][BF_4]$ and $[C_8mim][BF_4]$) are larger than those in DILs ($[C_{12}(mim)_2](BF_4)_2$ and $[C_{16}(mim)_2](BF_4)_2$). It is worthwhile to note that in this work, to compare chain length effects on the structural segregation of DILs and MILs in a rigorous way, MILs with varying alkyl tail lengths are chosen, where each alkyl tail chain length corresponds to one-half of the linkage chain length in DILs (i.e., $[C_nmim][BF_4]$ (n = 3, 6, 8) versus $[C_n(mim)_2](BF_4)_2$ (n = 6, 12, 16)).

To quantify the spatial heterogeneity observed in Figure 3, the HOPs for both DILs and MILs were calculated and shown in Figure 4. According to the study by Voth's group,[37] the HOP

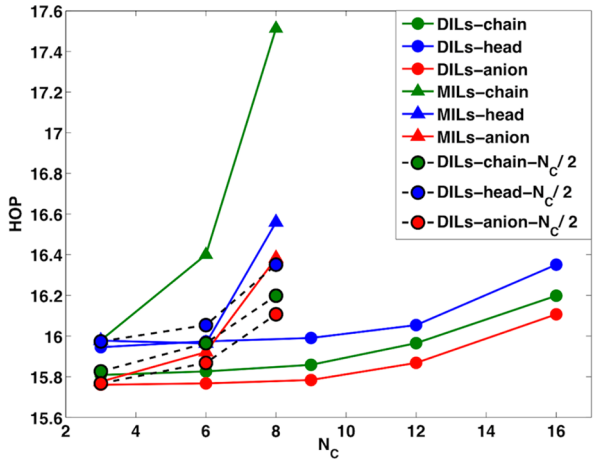

Figure 4. Heterogeneity order parameter (HOP) for alkyl chains (green), head groups (blue), and anions (red) of DILs (solid circles) and MILs (solid triangles) as a function of chain length (N_C, the number of $-CH_2$ in alkyl chain). The solid circles with black dash lines are HOP values of DILs with $N_C = N/2$ (N = 6, 12, 16; N is the number of $-CH_2$ in the alkyl chain of DILs). The carbon atom in the end of the alkyl tail chain of MILs and the carbon atoms in the middle of the linkage chain for DILs represent the alkyl chain site (for the even-numbered DILs, the site is defined as the center of mass of the two central carbon atoms in an alkyl linkage chain); the center of mass of head groups and anions were used to denote the anion sites and head sites, respectively.

value for homogenously distributed ideal particles is ~15.74. All the HOPs shown in Figure 4 are above 15.74, indicating the heterogeneous system for both DILs and MILs. Moreover, the HOP value increases with the elongation of the alkyl chain length in both DILs and MILs, indicating the increased structural segregation as chain length increases. This trend is in agreement with previous reports on MILs.[37,38] Nevertheless, the alkyl chains of MILs exhibit much larger HOP values compared with those in DILs, implying the higher degree of alkyl chain aggregation in MILs, which is evident by visual inspection of the snapshots shown in Figure 3. In addition, it is

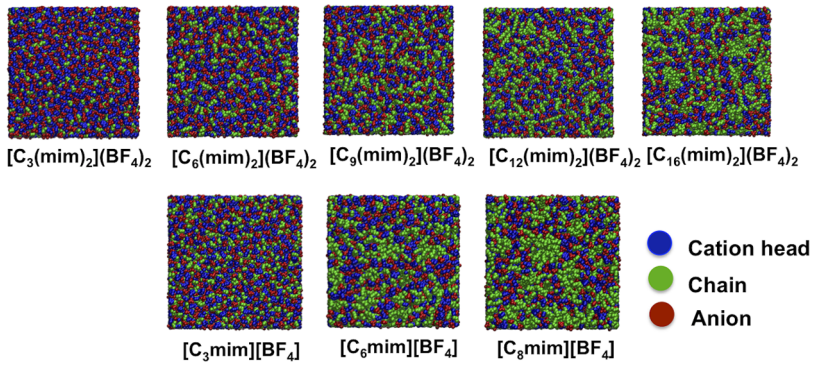

Figure 3. Snapshot of MD simulation of bulk dicationic $[C_n(mim)_2](BF_4)_2$ (n = 3, 6, 9, 12, 16) and monocationic $[C_nmim][BF_4]$ (n = 3, 6, 8). Cation head represents the imidazolium ring with its connected methyl group, and the remainder is classified as the chain.

dx.doi.org/10.1021/jp406381g | J. Phys. Chem. C 2013, 117, 18251−18257

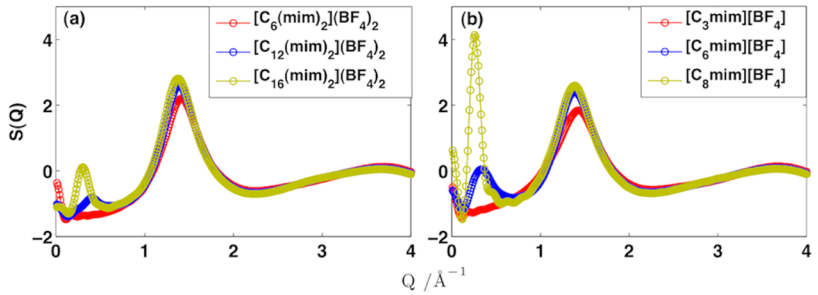

Figure 5. Total static structure factors for dicationic $[C_n(mim)_2](BF_4)_2$ (n = 6, 12, 16) (a) and monocationic $[C_nmim][BF_4]$ (n = 3, 6, 8) (b).

noteworthy that the alkyl chains of MILs display the highest HOP values compared with anions and head groups, whereas in DILs, the head groups exhibit the largest HOP, which underscores the fundamental structural differences between DILs and MILs. However, on average, the HOPs for DILs are dramatically lower than those of MILs.

To understand the different heterogeneities between DILs and MILs, the structural discrepancy between DILs and MILs is also analyzed through their total static structure functions shown in Figure 5. It is observed that for short-chain dicationic $[C_6(mim)_2](BF_4)_2$ and monocationic $[C_3mim][BF_4]$, almost the identical structure functions are present, both of which exhibit only one peak located at 1.4 $Å^{-1}$. The similarity is also found in their partial structure functions shown in Figure S2 (a and b) (Supporting Information). For chain lengths in the medium range ($[C_{12}(mim)_2](BF_4)_2$ versus $[C_6mim][BF_4]$), the discrepancy in prepeaks at 0.3 $Å^{-1}$ is evident; monocationic $[C_6mim][BF_4]$ displays a noticeable prepeak above the baseline, whereas the corresponding prepeak in the structure function of dicationic $[C_{12}(mim)_2](BF_4)_2$ is much less pronounced. Previous studies by Bodo[30] and Ishida et al.[29] claimed very similar structure factors between MILs and DILs, which is due to the short alkyl chains of cations investigated.

The analysis of the partial structure functions in Figure S2 (c and d) (Supporting Information) reveals that in monocationic $[C_6mim][BF_4]$ both anion−anion and cation−anion correlations contribute to the prepeak, whereas the prepeak in dicationic $[C_{12}(mim)_2](BF_4)_2$ stems from the anion−anion correlation exclusively. Such a trend becomes more evident for the long-chain dicationic $[C_{16}(mim)_2](BF_4)_2$ and monocationic $[C_8mim][BF_4]$ (Figure S2c,d, Supporting Information). We note that the anion−anion interaction is greatly strengthened in MILs in comparison to DILs. Also, the positive contribution of cation−anion correlations in MILs manifests itself as a negative contribution to the total $S(Q)$ in DILs. The partitioned cation head−anion and chain−anion subcomponents of cation−anion correlations in Figure S3 (Supporting Information) show that the contribution of cation head−anion correlation to the prepeak in DILs is largely canceled by the trough in the chain−anion structure function. The combined effect of cation head−anion and chain−anion correlations causes the dramatically increased prepeak in monocationic $[C_8mim][BF_4]$, which is associated with the enhanced structural heterogeneity.

According to Hettige et al.'s study,[28] it was concluded that the positive−negative (i.e., cation−anion) or polar−polar/apolar−apolar (i.e., polar head−head or anion−anion and apolar chain−chain) interaction gives rise to the length scale for the charge or polarity alternations, which suggests that the size of the nanoaggregates may be understood by considering the nonpolar alkyl chains. Figure 6 presents the cation head−anion

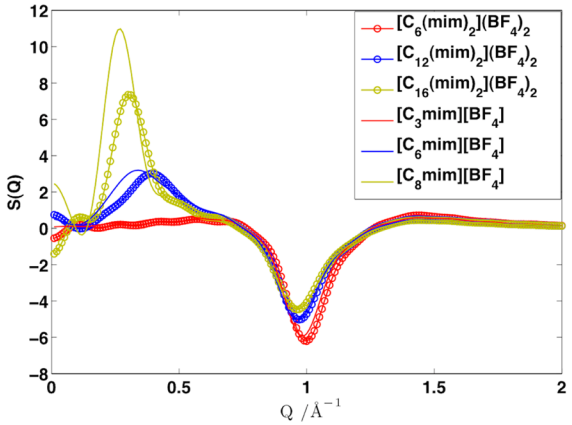

Figure 6. Comparison of cation head−anion subcomponents of DILs $[C_n(mim)_2](BF_4)_2$ (n = 6, 12, 16) and MILs $[C_nmim][BF_4]$ (n = 3,6,8), which implies the real space distance for polarity alternations.

subcomponents for both DILs and MILs in the series. Since it is reported that the positive prepeak identifies the length scale of polarity alternation and a negative peak (antipeak) at approximately 1.0 $Å^{-1}$ identifies that of charge alternations,[45] it is clear that the DILs in Figure 6 exhibit charge alternation distance similar to their counterparts of MILs but a polarity alternation distance shorter than that of MILs. Combined with the visual observation in Figure 3, it is rational to conclude that the nanoaggregate size formed by the alkyl chain is perhaps correlated with the length scale of polarity alternation in both DILs and MILs. The lower-Q prepeak position in MILs corresponds to the larger aggregate size and more significant structural heterogeneity.

The greater structural segregation in MILs is also supported by Baltazar et al.'s experiment.[46] In their study, the critical micelle concentration (CMC) values of a series of monocationic ($[C_nBIm][Br]$ (n = 8, 10, 12)) and dicationic ionic liquids ($[C_n(BIm)_2](Br)_2$ (n = 8, 10, 12)) were measured, and they found that the CMC decreases with increasing alkyl chain length of both MILs and DILs. The interesting finding is the dramatic decrease of the CMC for long-chain MILs, whereas DILs exhibit a more moderate decrease, suggesting the favorable aggregation for long-chain MILs but relatively unfavorable aggregation for DILs. Although the nanoscale aggregation for ILs in aqueous solutions is not exactly the same as that in neat ionic liquids, the similar trend predicted from this work invites further experimental explorations on this issue. The distinct structural nano-organizations for the aggregates formed in long-chain MILs and DILs will be discussed below.

The dominant role of anions in the structure of MILs has been demonstrated in Hettige et al.'s study.[28] To examine the

dx.doi.org/10.1021/jp406381g | J. Phys. Chem. C 2013, 117, 18251−18257

role of anions in DILs compared to MILs, different types of anions are employed, and their structure functions are shown in Figure 7. A variety of anions give rise to various structure

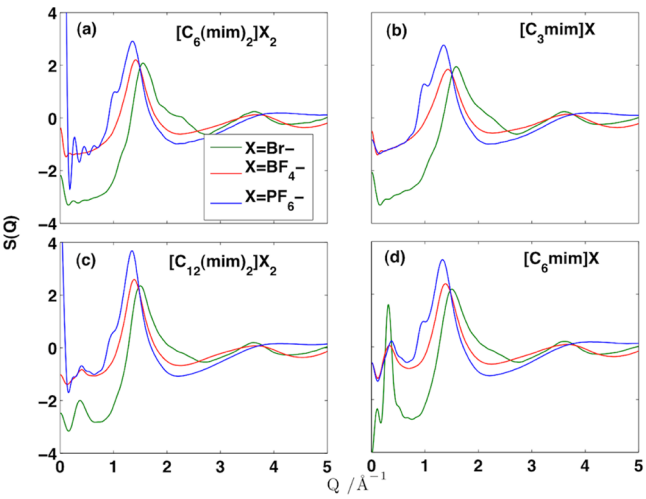

Figure 7. Anion-featured total static structure factors for dicationic $[C_n(mim)_2](X)_2$ (n = 6, 12 and X = Br, BF_4, PF_6) (a and c) and monocationic $[C_n mim][X]$ (n = 3, 6 and X = Br, BF_4, PF_6) (b and d).

functions for both long- and short-chain MILs and DILs. For short-chain $[C_6(mim)_2](X)_2$ and $[C_3mim][X]$, the peaks in their structure functions have almost identical amplitudes (ignoring the noise present at $Q < 0.15$ Å^{-1}), which is also substantiated in their partial structure functions in Figure S4 (Supporting Information). For long-chain $[C_{12}(mim)_2](X)_2$ and $[C_6mim][X]$, a discrepancy evident in the prepeaks is located at approximately 0.3 Å^{-1}. Br-containing MILs generate the most noticeable prepeaks followed by PF_6- and BF_4-containing MILs, stemming from the variety of the anion X-ray form factors. Their partial structure factors are shown in Figure S5 (Supporting Information), which reveals that anion−anion correlation contributes most to the prepeak in MILs and DILs regardless of the anion type. In particular, cation−anion interactions also contribute to the prepeak in MILs in contrast to DILs.

Now let us look into the structural nano-organization of long-chain MILs and DILs. Triolo et al. have proposed a micelle-like nanoaggregate model for MILs with long alkyl tails[23,42] as shown in Figure 8a, in which the free alkyl tails in the center interact with each other by van der Waals interaction and anions are excluded due to the strong electrostatic

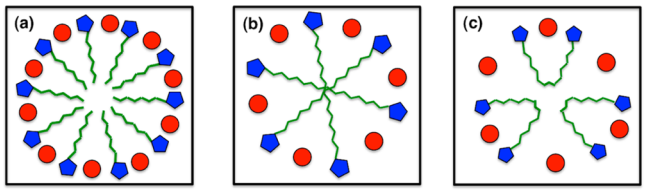

Figure 8. Schematic representation of the micelle-like nanoaggregates formed by a long alkyl tail in MILs proposed by Triolo et al.[23,44] (a) in contrast to the straight (b) and folded chain (c) models for the nanoscale arrangement of DILs with long linkage chain, respectively. The red dot represents the anion; the blue one denotes the positively charged ring; and the green line is the alkyl chain. Note that there are two anions for each cation in (b) and (c).

interaction between cation head groups and anions. For DILs, the nanoscale organization is more complicated since the linkage alkyl chain is constrained by the imidazolium ring at two ends, leading to the decreased flexibility. Therefore, it is relatively unfavorable for DILs with long linkage chains to assemble compared with their monocationic counterparts with free long tails. Deng et al.'s study[47] revealed that the replacement of the terminal $-CH_3$ group with the $-OH$ group in the alkyl chain of MILs results in the failure of aggregation of long alkyl tails. A similar consequence occurring in DILs may result from the enhanced polarity compared with MILs by additional polar head groups in dications, which prevents the evident aggregation of nonpolar alkyl chains. This is also evidenced by the shorter polarity alternation distance of DILs in contrast to MILs shown in Figure 6. The smaller-sized aggregates observed in DILs indicate fewer DILs are involved in the aggregate formation because of the increased polarity resulting from additional polar head groups.

Moreover, the relative distance of the two imidazolium rings may also play a big role during the aggregation of long-chain DILs. In this case, there are two models proposed for the assembly of long linkage chains in DILs, which are shown in Figure 8b,c. One is the straight chain model (Figure 8b), in which straight linkage chains cross with each other in the center of the micelle with the two completely separated positively charged rings surrounded by negatively charged anions. The other folded chain model (Figure 8c) describes the situation when two rings are close to each other through a highly curved linkage chain. However, the distribution of the angle formed by the two vectors pointing from each ring of the dication to the center of the linkage chains, shown in Figure 9a, demonstrates that the folded chain model is not preferred in DILs since the long-chain dications exhibit the highest population in large obtuse angles, which suggests the dication tends to be in an unfolded state. The angle with the largest population as a function of chain length shown in Figure 9b exhibits a bell-like relationship, which can be interpreted as the interplay between the polarity alternation and the increased flexibility with the elongation of alkyl chains. For short-chain dications, the shorter distance between polar groups (head groups and anions) results in the stronger electrostatic interaction between head groups and anions, which may highly fold the chain with sharp angles; with the increase in chain length, the polarity alternation distance is increased, which strengthens the unfolding of alkyl chains. However, as the chain length increases, the chain flexibility is enhanced as well. The maximum angle was reached as the polarity alternation dominates (as n = 9), whereas the chain flexibility increases and the influence of the chain flexibility overwhelms the increased polarity alternation, which leads to the folding of alkyl chains again. The dependence of angle distribution on anions was shown in Figure S6 (Supporting Information), which presents weak dependence on the type of anions. This may be due to the smaller sizes of anions chosen in simulations in contrast to the sizes of dications or the shapes and components of anions, which need further investigation in the future.

It should be noted that the models shown in Figure 8b,c do not correspond to the angular distribution function in Figure 9a. The straight chain model represents the highly unfolded state or wide-angle region in Figure 9a, and the folded chain model corresponds to the tightly folded state or narrow angle region. Although Figure 8b presents the favorable nano-aggregate structure for long-chain dications, it is noteworthy

dx.doi.org/10.1021/jp406381g | J. Phys. Chem. C 2013, 117, 18251−18257

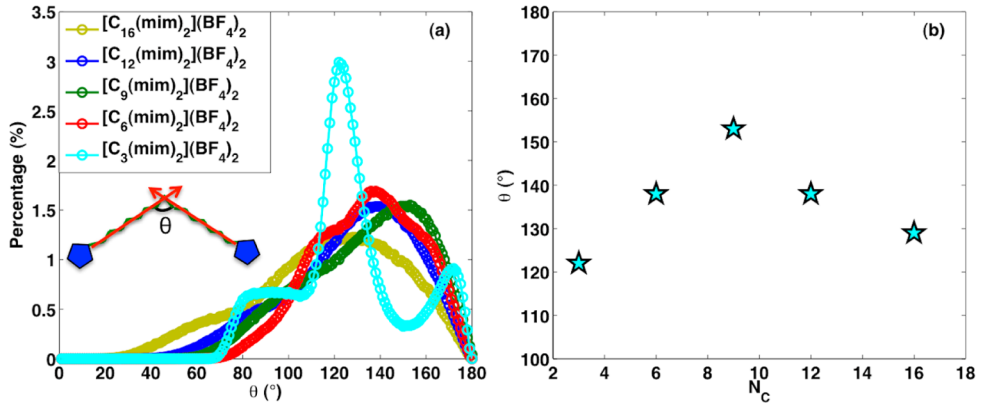

Figure 9. (a) Distribution of the angle formed by two vectors pointing from the ring to the center atoms of the linkage chain in $[C_n(mim)_2](BF_4)_2$ (n = 3, 6, 8, 12, 16). (b) The angle with the largest population (the angle corresponding to the maximum percentage show in (a)) as a function of linkage chain length.

that these two models describe the idealized cases; in reality the nanoscale aggregates are more complicated and may consist of the mixture of a majority of unfolded (as shown in Figure 8b) and a small portion of highly folded (as shown in Figure 8c) DILs. Compared with the linkage chains of DILs with restrained flexibility, the flexible alkyl tails in MILs are likely able to aggregate with each other under the driving of van der Waals interactions, which is reflected in the more significant structural heterogeneities in MILs.

4. CONCLUSION

In conclusion, this work unravels the different behaviors in structural arrangement of the alkyl linkage chain of DILs at long-, medium-, and short-range lengths in comparison with the alkyl tail chains of MILs. For the short-range alkyl chain, the cations in DILs and MILs exhibit nearly identical structural nano-organization and heterogeneity; the significant difference in structural heterogeneity of DILs and MILs is observed in medium-/long-chain ILs regardless of the type of anions, which is supported by the HOP values as well. The unique assembly pattern for long linkage chains (straight and folded chain models) in DILs explains the observed insignificance of prepeaks contrary to those in MILs, which provides molecular insights into the nature of structural heterogeneity in DILs as well as a conceptual model for the interpretation of experimental observations.

■ ASSOCIATED CONTENT

Supporting Information

Figure S1 shows the radial distribution function for DILs. Figures S2–S5 provide a comparison of partial structure functions between DILs and MILs. The angle distribution function of DILs with different anions is shown in Figure S6. This material is available free of charge via the Internet at http://pubs.acs.org.

■ AUTHOR INFORMATION

Corresponding Author

*E-mail: guang.feng@vanderbilt.edu; peter.cummings@vanderbilt.edu. Telephone: 1-864-633-8419.

Notes

The authors declare no competing financial interest.

■ ACKNOWLEDGMENTS

This work was supported as part of the Fluid Interface Reactions, Structures, and Transport (FIRST) Center, an Energy Frontier Research Center funded by the U.S. Department of Energy, Office of Science, Office of Basic Energy Sciences. We acknowledge the National Energy Research Scientific Computing Center, which is supported by the Office of Science of the U.S. Department of Energy under Contract No. DE-AC02-05CH11231. G.F. also appreciates the Palmetto cluster at Clemson University for providing computer time.

■ REFERENCES

(1) Forsyth, S. A.; Pringle, J. M.; MacFarlane, D. R. Ionic Liquids - An Overview. *Aust. J. Chem.* **2004**, *57*, 113–119.
(2) Yoshizawa, M.; Ito-Akita, K.; Ohno, H. Evidence of Inter-Action between Anion and Polyether in the Bulk. *Electrochim. Acta* **2000**, *45*, 1617–1621.
(3) Anderson, J. L.; Ding, R. F.; Ellern, A.; Armstrong, D. W. Structure and Properties of High Stability Geminal Dicationic Ionic Liquids. *J. Am. Chem. Soc.* **2005**, *127*, 593–604.
(4) Fang, D.; Yang, J. M.; Ni, C. J. Dicationic Ionic Liquids as Recyclable Catalysts for One-Pot Solvent-Free Synthesis of Alpha-Aminophosphonates. *Heteroatom. Chem.* **2011**, *22*, 5–10.
(5) Chinnappan, A.; Kim, H. Environmentally Benign Catalyst: Synthesis, Characterization, and Properties of Pyridinium Dicationic Molten Salts (Ionic Liquids) and Use of Application in Esterification. *Chem. Eng. J.* **2012**, *187*, 283–288.
(6) Fan, M. M.; Yang, J.; Jiang, P. P.; Zhang, P. B.; Li, S. S. Synthesis of Novel Dicationic Basic Ionic Liquids and Its Catalytic Activities for Biodiesel Production. *RSC Adv.* **2013**, *3*, 752–756.
(7) Liu, X. F.; Xiao, L. F.; Wu, H. J. T.; Chen, J.; Xia, C. G. Synthesis of Novel Gemini Dicationic Acidic Ionic Liquids and Their Catalytic Performances in the Beckmann Rearrangement. *Helv. Chim. Acta* **2009**, *92*, 1014–1021.
(8) Han, X. X.; Armstrong, D. W. Using Geminal Dicationic Ionic Liquids as Solvents for High-Temperature Organic Reactions. *Org. Lett.* **2005**, *7*, 4205–4208.
(9) Pagano, F.; Gabler, C.; Zare, P.; Mahrova, M.; Dorr, N.; Bayon, R.; Fernandez, X.; Binder, W. H.; Hernaiz, M.; Tojo, E.; Igartua, A. Dicationic Ionic Liquids as Lubricants. *Proc. Inst. Mech. Eng., Part J* **2012**, *226*, 952–964.
(10) Jin, C. M.; Ye, C. F.; Phillips, B. S.; Zabinski, J. S.; Liu, X. Q.; Liu, W. M.; Shreeve, J. M. Polyethylene Glycol Functionalized Dicationic Ionic Liquids with Alkyl or Polyfluoroalkyl Substituents as High Temperature Lubricants. *J. Mater. Chem.* **2006**, *16*, 1529–1535.

(11) Zhancy, Z. X.; Zhou, H.; Yang, L.; Tachibana, K.; Kamijima, K.; Xu, J. Asymmetrical Dicationic Ionic Liquids Based on Both Imidazolium and Aliphatic Ammonium as Potential Electrolyte Additives Applied to Lithium Secondary Batteries. *Electrochim. Acta* **2008**, *53*, 4833−4838.
(12) Cho, W. J.; Yeom, C. G.; Kim, B. C.; Kim, K. M.; Ko, J. M.; Yu, K. H. Supercapacitive Properties of Activated Carbon Electrode in Organic Electrolytes Containing Single- and Double-Cationic Liquid Salts. *Electrochim. Acta* **2013**, *89*, 807−813.
(13) Davis, J. H. Task-Specific Ionic Liquids. *Chem. Lett.* **2004**, *33*, 1072−1077.
(14) Castner, E. W., Jr.; Margulis, C. J.; Maroncelli, M.; Wishart, J. F. Ionic Liquids: Structure and Photochemical Reactions. *Annu. Rev. Phys. Chem.* **2011**, *62*, 85−105.
(15) Tsuda, T.; Hussey, C. L. Electrochemical Applications of Room-Temperature Ionic Liquids. *Electrochem. Soc. Interface* **2007**, *16*, 42−49.
(16) Lall, S. I.; Mancheno, D.; Castro, S.; Behaj, V.; Cohen, J. L. I.; Engel, R. Polycations. Part X. Lips, a New Category of Room Temperature Ionic Liquid Based on Polyammonium Salts. *Chem. Commun.* **2000**, 2413−2414.
(17) Payagala, T.; Huang, J.; Breitbach, Z. S.; Sharma, P. S.; Armstrong, D. W. Unsymmetrical Dicationic Ionic Liquids: Manipulation of Physicochemical Properties Using Specific Structural Architectures. *Chem. Mater.* **2007**, *19*, 5848−5850.
(18) Karna, M.; Lahtinen, M.; Hakkarainen, P. L.; Valkonen, J. Physicochemical Properties of New Dicationic Ether-Functionalized Low Melting Point Ammonium Salts. *Aust. J. Chem.* **2010**, *63*, 1122−1137.
(19) Shirota, H.; Ishida, T. Microscopic Aspects in Dicationic Ionic Liquids through the Low-Frequency Spectra by Femtosecond Raman-Induced Kerr Effect Spectroscopy. *J. Phys. Chem. B* **2011**, *115*, 10860−10870.
(20) Shirota, H.; Mandai, T.; Fukazawa, H.; Kato, T. Comparison between Dicationic and Monocationic Ionic Liquids: Liquid Density, Thermal Properties, Surface Tension, and Shear Viscosity. *J. Chem. Eng. Data* **2011**, *56*, 2453−2459.
(21) Annapureddy, H. V. R.; Kashyap, H. K.; Biase, P. M.; Margulis, C. J. What Is the Origin of the Prepeak in the X-Ray Scattering of Imidazolium-Based Room-Temperature Ionic Liquids? *J. Phys. Chem. B* **2010**, *114*, 16838−16846.
(22) Bradley, A. E.; Hardacre, C.; Holbrey, J. D.; Johnston, S.; McMath, S. E. J.; Nieuwenhuyzen, M. Small-Angle X-Ray Scattering Studies of Liquid Crystalline 1-Alkyl-3-methylimidazolium Salts. *Chem. Mater.* **2002**, *14*, 629−635.
(23) Triolo, A.; Russina, O.; Fazio, B.; Triolo, R.; Di Cola, E. Morphology of 1-Alkyl-3-Methylimidazolium Hexafluorophosphate Room Temperature Ionic Liquids. *Chem. Phys. Lett.* **2008**, *457*, 362−365.
(24) Hardacre, C.; Holbrey, J. D.; Mullan, C. L.; Youngs, T. G.; Bowron, D. T. Small Angle Neutron Scattering from 1-Alkyl-3-Methylimidazolium Hexafluorophosphate Ionic Liquids ([C(N)Mim][Pf(6)], N = 4, 6, and 8). *J. Chem. Phys.* **2010**, *133*, 074510.
(25) Wang, Y.; Voth, G. A. Unique Spatial Heterogeneity in Ionic Liquids. *J. Am. Chem. Soc.* **2005**, *127*, 12192−12193.
(26) Urahata, S. M.; Ribeiro, M. C. Structure of Ionic Liquids of 1-Alkyl-3-methylimidazolium Cations: A Systematic Computer Simulation Study. *J. Chem. Phys.* **2004**, *120*, 1855−1863.
(27) Margulis, C. J. Computational Study of Imidazolium-Based Ionic Solvents with Alkyl Substituents of Different Lengths. *Mol. Phys.* **2004**, *102*, 829−838.
(28) Hettige, J. J.; Kashyap, H. K.; Annapureddy, H. V. R.; Margulis, C. J. Anions, the Reporters of Structure in Ionic Liquids. *J. Phys. Chem. Lett.* **2013**, *4*, 105−110.
(29) Ishida, T.; Shirota, H. Dicationic Versus Monocationic Ionic Liquids: Distinctive Ionic Dynamics and Dynamical Heterogeneity. *J. Phys. Chem. B* **2013**, *117*, 1136−1150.
(30) Bodo, E.; Chiricotto, M.; Caminiti, R. Structure of Geminal Imidazolium Bis(trifluoromethylsulfonyl)Imide Dicationic Ionic Liquids: A Theoretical Study of the Liquid Phase. *J. Phys. Chem. B* **2011**, *115*, 14341−14347.
(31) Yeganegi, S.; Soltanabadi, A.; Farmanzadeh, D. Molecular Dynamic Simulation of Dicationic Ionic Liquids: Effects of Anions and Alkyl Chain Length on Liquid Structure and Diffusion. *J. Phys. Chem. B* **2012**, *116*, 11517−11526.
(32) Lopes, J. N. C.; Deschamps, J.; Padua, A. A. H. Modeling Ionic Liquids Using a Systematic All-Atom Force Field. *J. Phys. Chem. B* **2004**, *108*, 2038−2047.
(33) Hess, B.; Bekker, H.; Berendsen, H. J. C.; Fraaije, J. G. E. M. Lincs: A Linear Constraint Solver for Molecular Simulations. *J. Comput. Chem.* **1997**, *18*, 1463−1472.
(34) Essmann, U.; Perera, L.; Berkowitz, M. L.; Darden, T.; Lee, H.; Pedersen, L. G. A Smooth Particle Mesh Ewald Method. *J. Chem. Phys.* **1995**, *103*, 8577−8593.
(35) Berendsen, H. J. C.; Vanderspoel, D.; Vandrunen, R. Gromacs - a Message-Passing Parallel Molecular-Dynamics Implementation. *Comput. Phys. Commun.* **1995**, *91*, 43−56.
(36) Borodin, O.; Gorecki, W.; Smith, G. D.; Armand, M. Molecular Dynamics Simulation and Pulsed-Field Gradient Nmr Studies of Bis(Fluorosulfonyl)Imide (FSI) and Bis[(Trifluoromethyl)Sulfonyl]-Imide (TFSI)-Based Ionic Liquids. *J. Phys. Chem. B* **2010**, *114*, 6786−6798.
(37) Wang, Y.; Voth, G. A. Tail Aggregation and Domain Diffusion in Ionic Liquids. *J. Phys. Chem. B* **2006**, *110*, 18601−18608.
(38) Ji, Y. M.; Shi, R.; Wang, Y. T.; Saielli, G. Effect of the Chain Length on the Structure of Ionic Liquids: From Spatial Heterogeneity to Ionic Liquid Crystals. *J. Phys. Chem. B* **2013**, *117*, 1104−1109.
(39) Li, S.; Banuelos, J. L.; Guo, J.; Anovitz, L.; Rother, G.; Shaw, R. W.; Hillesheim, P. C.; Dai, S.; Baker, G. A.; Cummings, P. T. Alkyl Chain Length and Temperature Effects on Structural Properties of Pyrrolidinium-Based Ionic Liquids: A Combined Atomistic Simulation and Small-Angle X-Ray Scattering Study. *J. Phys. Chem. Lett.* **2012**, *3*, 125−130.
(40) Santos, C. S.; Murthy, N. S.; Baker, G. A.; Castner, E. W. Communication: X-Ray Scattering from Ionic Liquids with Pyrrolidinium Cations. *J. Chem. Phys.* **2011**, *134*.
(41) Kashyap, H. K.; Santos, C. S.; Annapureddy, H. V. R.; Murthy, N. S.; Margulis, C. J.; Castner, E. W. Temperature-Dependent Structure of Ionic Liquids: X-Ray Scattering and Simulations. *Faraday Discuss.* **2012**, *154*, 133−143.
(42) Russina, O.; Triolo, A.; Gontrani, L.; Caminiti, R.; Xiao, D.; Larry, G. H., Jr.; Bartsch, R. A.; Quitevis, E. L.; Plechkova, N.; Seddon, K. R. Morphology and Intermolecular Dynamics of 1-Alkyl-3-Methylimidazolium Bis{(Trifluoromethane)Sulfonyl}Amide Ionic Liquids: Structural and Dynamic Evidence of Nanoscale Segregation. *J. Phys.: Condens. Matter* **2009**, *21*, 424121.
(43) Saboungi, M. L.; Aoun, B.; Goldbach, A.; Gonzalez, M. A.; Kohara, S.; Price, D. L. Nanoscale Heterogeneity in Alkyl-Methylimidazolium Bromide Ionic Liquids. *J. Chem. Phys.* **2011**, *134*, 104509.
(44) Triolo, A.; Russina, O.; Bleif, H. J.; Di Cola, E. Nanoscale Segregation in Room Temperature Ionic Liquids. *J. Phys. Chem. B* **2007**, *111*, 4641−4644.
(45) Kashyap, H. K.; Hettige, J. J.; Annapureddy, H. V. R.; Margulis, C. J. Saxs Anti-Peaks Reveal the Length-Scales of Dual Positive-Negative and Polar−Apolar Ordering in Room-Temperature Ionic Liquids. *Chem. Commun.* **2012**, *48*, 5103−5105.
(46) Baltazar, Q. Q.; Chandawalla, J.; Sawyer, K.; Anderson, J. L. Interfacial and Micellar Properties of Imidazolium-Based Monocationic and Dicationic Ionic Liquids. *Colloid Surf. A* **2007**, *302*, 150−156.
(47) Deng, L.; Shi, R.; Wang, Y. T.; Ou-Yang, Z. C. Hydrogen-Bond Rich Ionic Liquids with Hydroxyl Cationic Tails. *Chem. Phys. Lett.* **2013**, *560*, 32−36.